Journal of Applied Mathematics and Physics, 2025, 13(7), 2245-2259
https://www.scirp.org/journal/jamp
ISSN Online: 2327-4379
ISSN Print: 2327-4352

Two-Dimensional Numerical Analysis of Multi-Caliber Drainage Pipe Impact Mechanism with Barrier on the Transition Process of Convective System

Guoxin Jiang[1], Junli Guo[1], Xin Zhang[1], Chunyi Zhuang[1], Zelong Ma[1], Chuan Zhao[1*], Shengjun Huang[2]

[1]Sichuan Academy of Water Conservancy, Chengdu, China
[2]Sichuan Xiangjiaba Irrigation Area Construction and Development Co., Ltd., Yibin, China
Email: *zhaochuanvip@163.com

How to cite this paper: Jiang, G.X., Guo, J.L., Zhang, X., Zhuang, C.Y., Ma, Z.L., Zhao, C. and Huang, S.J. (2025) Two-Dimensional Numerical Analysis of Multi-Caliber Drainage Pipe Impact Mechanism with Barrier on the Transition Process of Convective System. *Journal of Applied Mathematics and Physics*, **13**, 2245-2259.
https://doi.org/10.4236/jamp.2025.137128

Received: June 20, 2025
Accepted: July 15, 2025
Published: July 18, 2025

Abstract

The water carrying capacity and head loss of pipelines are significantly affected by the flow state, aiming at the problem that the transition flow characteristics of multi caliber basalt fiber drainage pipe are not clear, based on the two-dimensional numerical simulation results of multi-diameter pipes with barriers, this paper systematically analyzes the transition path and transition mechanism of the multi-diameter drainage pipe convection system under the action of barriers in the range of $Re = 10^3 - 2.73 \times 10^8$. The results show that: 1) The main mode solution of multi-aperture basalt fiber drainage pipe convection system is steady flow in the process of transition to chaos. 2) Compared with the non-barrier condition, the transition process of the multi-aperture basalt fiber drainage pipe with the barrier is obviously delayed, that is, the critical Reynolds number of the convective system evolving from laminar flow to turbulent flow is larger. The research results show that the design of the barrier can effectively improve the water conveyance capacity of the pipeline, which can provide reference for the optimal design of multi-diameter drainage pipes.

Keywords

Basalt Fiber Drainage Pipe, Transitional Flow, Flow Restrictor, Reynolds Number

1. Introduction

As a new type of environmental protection pipeline material, basalt fiber drainage

pipe plays an important role in municipal, construction, chemical and other fields with its excellent performance of high strength, corrosion resistance and environmental protection. However, the turbulent mixing effect of multi-diameter basalt fiber drainage pipe at the intersection of flow is strong. For the laminar flow of differential pressure driven drainage pipe flow, it is stable to small amplitude disturbance (linear disturbance) at medium Reynolds number [1], but when the disturbance amplitude is large enough, it can become turbulent, that is, subcritical transition occurs [2] [3]. Compared with laminar flow, the momentum, energy and mass transfer characteristics of turbulent flow are very different. In turbulent state, water flow needs to overcome greater friction resistance [4]. The energy loss is greater and has a direct impact on the flow capacity. Therefore, it is of great engineering significance to inhibit the transition of water flow from laminar flow to turbulent flow in the drainage pipe to improve the flow capacity of the drainage pipe.

Transition refers to the process of transition from laminar flow to turbulent flow, which is a common phenomenon in production and life. The study of transition flow has important theoretical and engineering significance in fluid mechanics. In recent years, the study of transition flow has attracted much attention in the field of turbulence control and energy optimization, especially the active intervention of turbulence to laminar flow in pipeline flow has become a hot spot. The traditional theory takes Reynolds number (Re) as the core criterion, and the critical Reynolds number of transition in pipeline flow is about 2300 [5]. However, according to the experimental research of subsequent scholars, it is found that transition may occur in a wider range of Reynolds number [6]-[9], and the critical Reynolds number can be as low as 1750 or as high as 23000, indicating that transition not only depends on Reynolds number, but also is closely related to flow disturbance, inlet conditions and pipeline geometric characteristics. Hattori [10] and Kanda [11] *et al.* showed that the momentum difference between laminar flow and turbulent flow is the key to trigger the transition. At high Reynolds number, the length of the turbulent development zone is shortened, resulting in the change of the flow state in the downstream transition zone. The transition boundary is weakly dependent on the aspect ratio of the tube, but the laminar or turbulent state in the inlet development zone will significantly affect the downstream transition process. The traditional critical Reynolds number ($Re \approx 2300$) corresponds to the onset of transition II, which is related to the boundary layer transition in the flow development zone. By precisely controlling the inlet velocity profile, laminar flow may still be maintained at high Reynolds numbers ($Re > 10{,}000$) [12] [13]. The study of Nishi [14] revealed the deterministic evolution of the local turbulent bubble Puffs and the continuous turbulent section Slugs. The results show that the transition not only depends on the Reynolds number, but also is closely related to the disturbance type, spatial position and pipeline development length.

In addition to the influence factors such as flow disturbance, inlet conditions and pipeline geometric characteristics, in recent years, scholars Küuhnen [15] and

Marensi [16] have proposed an innovative method based on steady-state control of streamwise velocity profile: by inserting fixed obstacles in the pipeline to change the flow field distribution, the flow velocity in the center of the pipeline is reduced and the near-wall region is accelerated. Experimental measurements show that when the Re ≤ 6000, the flow can be completely re-layered and the downstream friction resistance is reduced to 34% of the turbulent state; even at high Re (Re ≈ 10,000), local transient re-laminarization can still be observed in the downstream of the device, accompanied by a phased reduction in frictional resistance. In summary, by inserting a fixed obstacle in the pipe, the turbulent regeneration cycle can be destroyed and the flow re-layering can be induced. The turbulence can be effectively suppressed by optimizing the flow disturbance mechanism [17].

2. Model and Work Condition

2.1. Model Construction

In this study, Fluent fluid calculation software was used to construct a multi-diameter basalt fiber drainage pipe convection system model and carry out relevant simulation calculations. The model is shown in **Figure 1**. The drainage pipe includes a main pipe and two side nozzles, and the side nozzles are connected to the main pipe through oblique nozzles. The main pipe is internally fixed with a barrier, and the longitudinal structural surface of the barrier is funnel-shaped. The computational domain of the computational model is 3D × 10D. The inlet boundary conditions of the main pipe and the side pipe are the velocity inlet, the outlet boundary condition of the main pipe is the pressure outlet, and the side wall of the channel and the bottom boundary outside the computational domain are the non-slip wall. And because the flow pattern is required to be high Re pipe flow, the turbulence model uses the k-ε model of the RANS. The working fluid in the drainage pipeline is water and remains isothermal at the initial time.

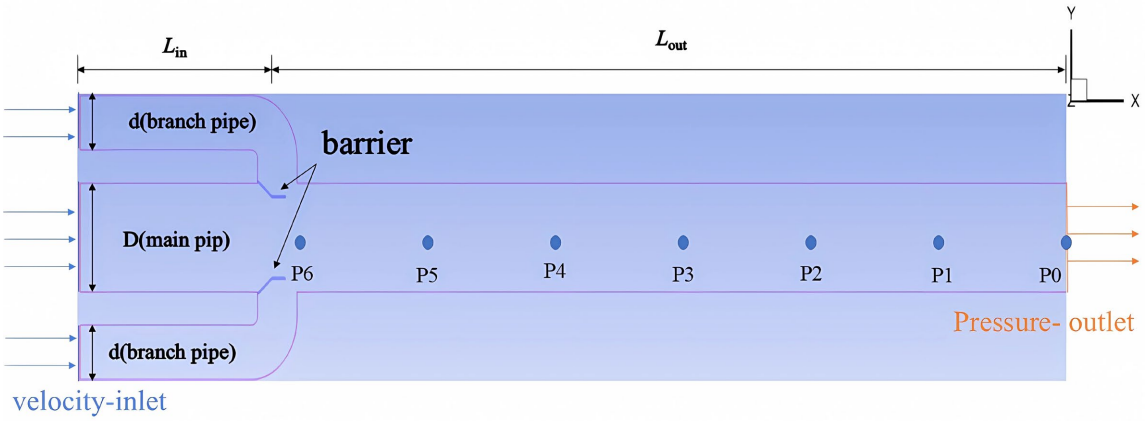

Figure 1. The model and boundary conditions of the multi-caliber basalt fiber drainage pipe convection system.

2.2. Governing Equation

The flow of the convective system of the multi-diameter basalt fiber drainage pipe

originates from the inflow of the main pipe and the side pipe of the drainage pipe, and the development of the flow can be described by the 2D N-S equation. The specific control equation is:

$$\frac{\partial u}{\partial x}+\frac{\partial v}{\partial y}=0 \tag{1}$$

$$\frac{\partial u}{\partial t}+u\frac{\partial u}{\partial x}+v\frac{\partial u}{\partial y}=-\frac{\partial p}{\partial x}+\nu\left(\frac{\partial^2 u}{\partial x^2}+\frac{\partial^2 u}{\partial y^2}\right) \tag{2}$$

$$\frac{\partial v}{\partial t}+u\frac{\partial v}{\partial x}+v\frac{\partial v}{\partial y}=-\frac{\partial p}{\partial y}+\nu\left(\frac{\partial^2 v}{\partial x^2}+\frac{\partial^2 v}{\partial y^2}\right) \tag{3}$$

The dimensionless control parameter Reynolds number Re is defined as follows:

$$\mathrm{Re}=\frac{v_{ave}D}{\nu} \tag{4}$$

2.3. Dependence Test

In order to ensure the accuracy of the constructed model, the calculation domain range side nozzle length × main pipe length ($L_{in} \times L_{out}$) is selected as 3D × 10D, the number of grids is 3×10^5, and the calculation step is 0.5s as the benchmark model. Grid dependence test, step dependence test and calculation domain dependence test are carried out. The control parameters are: the ratio of side pipe to main pipe diameter A_1:A_2 = 1:2, Prandtl number Pr = 7, Re = 6×10^7.

1) Model grid dependency testing

The fixed calculation domain ($L_{in} \times L_{out}$) is 3D × 10D and the calculation step is 0.5s. The number of design grids is 1.5×10^5, 3.0×10^5 and 6.0×10^5. The grid accuracy is tested, and the monitoring point P_2 is used as the observation object. The fully developed velocity time series of the three groups of grid calculations is shown in Figure 2, and the statistical data is shown in Table 1.

It can be seen from Figure 2 and Table 1 that at the monitoring point P_2, the velocity signals of the two sets of grids of 3.0×10^5 and 6.0×10^5 are basically consistent, but there is an obvious phase difference. The average quantitative analysis results of the full development of the two sets of grids can be seen in Table 1, and the average error is less than 0.02%.

Table 1. The statistics of the $v_{x,ave}$ for different grid quantities at P_2.

Grid number	Time step (s)	Computational domain	$v_{x,ave}$ (m/s)	Error
1.5×10^5	0.5	3D × 10D	333.42	0.02%
3.0×10^5	0.5	3D × 10D	333.75	-
6.0×10^5	0.5	3D × 10D	333.72	0.01%

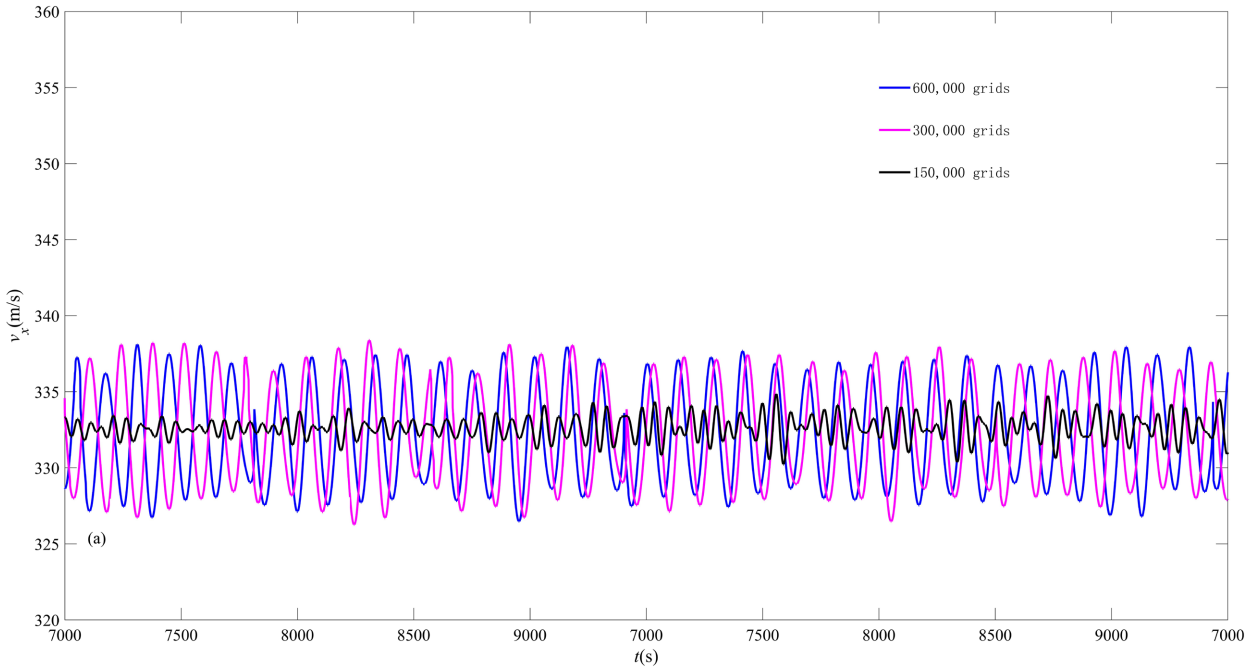

Figure 2. The $v_{x,ave}$ for different grid quantities at P_2.

2) Time step dependence test

The fixed computational domain ($L_{in} \times L_{out}$) is 3D × 10D and the number of grids is 600,000. Three time steps of 0.25 s, 0.5 s and 1.0 s are designed for dependency test. The monitoring point P_2 is taken as the observation object. The velocity time series under the three time steps are shown in **Figure 3**. The statistical data are shown in **Table 2**.

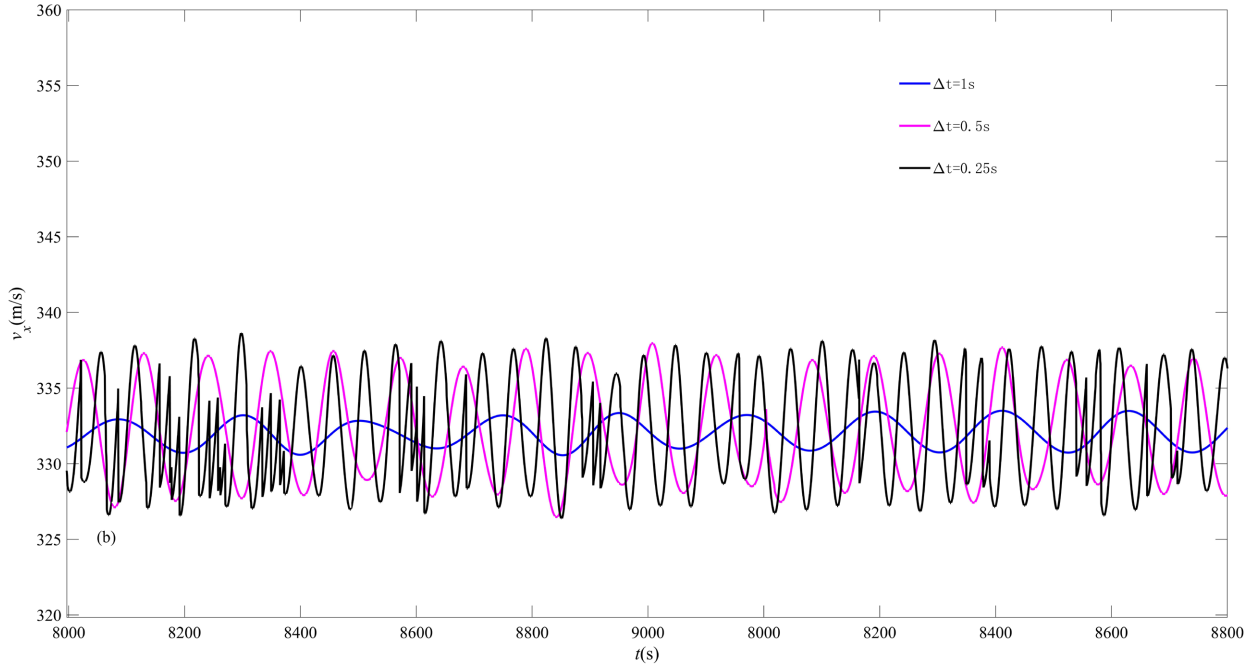

Figure 3. The $v_{x,ave}$ for different calculation time steps at P_2.

Table 2. The statistics of the $v_{x,ave}$ for different calculation time steps at P_2.

Grid number	Time step (s)	Computational domain	$v_{x,ave}$ (m/s)	error
6.0×10^5	0.25	3D × 10D	333.75	0.00%
6.0×10^5	0.5	3D × 10D	333.75	-
6.0×10^5	1.0	3D × 10D	333.78	0.02%

It can be seen from Figure 3 and Table 2 that at the monitoring point P_2, there are obvious differences in the velocity signals of the two groups of time steps of 0.25 s and 0.5 s. The average error of the full development of the two groups of time steps of 0.5 s and 1 s is less than 0.02%.

3) Computational domain dependency testing

In addition, the dependence of the numerical simulation results on the computational domain is tested, based on three computational domains of 3D × 10D, 6D × 10D and 3D × 20D. The average error of the temperature at the fully developed fixed point obtained by different computational domains is shown in Table 3, and the error is less than 0.04%.

Table 3. The statistics of the $v_{z,ave}$ for different computational domains at P_2.

Time step (s)	Computational domain	$v_{z,ave}$	Error
0.25	3D × 10D	333.75	-
0.5	6D × 10D	333.92	0.04%
1.0	3D × 20D	333.83	0.03%

In summary, based on the double consideration of calculation accuracy and calculation amount, the 3D × 10D calculation domain, the number of grids 6.0×10^5, and the calculation step length 0.5 s are finally selected. The model uses an unstructured tetrahedral mesh, and the mesh at the inlet of the pipe velocity, the barrier and the pipe wall is locally encrypted, that is, a finer mesh is used, and the mesh is shown in Figure 4.

Figure 4. Meshing of multi-orifice basalt fiber drains with barriers.

Table 4. Calculate the list of work condition.

Connection mode	Re	Main pipe flow rate vm (m/s)	Side pipe flow rate vs (m/s)	Flow Q (m^3/s)
Barrier	2.73×10^8	100	100	60
	1.64×10^8	60	60	36
	1.09×10^8	40	40	24
	8.2×10^6	3	3	1.8
	6.15×10^6	3	1.5	1.35
	7.65×10^6	2.8	2.8	1.68
	7.1×10^6	2.6	2.6	1.56
	6.56×10^6	2.4	2.4	1.44
	6×10^6	2.2	2.2	1.32
	5.46×10^6	2	2	1.2
	4.1×10^6	2	1	0.9
	4.92×10^6	1.8	1.8	1.08
	4.37×10^6	1.6	1.6	0.96
	3.82×10^6	1.4	1.4	0.84
	3.28×10^6	1.2	1.2	0.72
	2.73×10^6	1	1	0.6
	2.05×10^6	1	0.5	0.45
	2.18×10^6	0.8	0.8	0.48
	1.64×10^6	0.6	0.6	0.36
	1.09×10^6	0.4	0.4	0.24
	5.46×10^5	0.2	0.2	0.12
	4.1×10^5	0.2	0.1	0.09
	2.3×10^3	8.34×10^{-4}	8.34×10^{-4}	4.433×10^{-4}
	10^3	3.63×10^{-4}	3.63×10^{-4}	2.217×10^{-4}
Non-barrier	8.2×10^6	3	3	1.8
	6.15×10^6	3	1.5	1.35
	5.46×10^6	2	2	1.2
	4.1×10^6	2	1	0.9
	2.73×10^6	1	1	0.6
	2.05×10^6	1	0.5	0.45
	5.46×10^5	0.2	0.2	0.12
	4.1×10^5	0.2	0.1	0.09
	2.3×10^3	8.34×10^{-4}	8.34×10^{-4}	4.433×10^{-4}
	10^3	3.63×10^{-4}	3.63×10^{-4}	2.217×10^{-4}

2.4. Calculated Work Condition

In this paper, the transition path of the convection system of the multi-diameter basalt fiber drainage pipe in the Reynolds number control parameter space is studied. The diameter ratio of the side main pipe is 1:2, the working medium is water, the Prandtl number is Pr = 7, the Re range is Re = 10^3 − 2.73 × 10^8, and the main side pipe connection is divided into two connection states whether there is a barrier or not.

The maximum allowable flow rate of the pipeline designed in this study is 3 m/s. After pre-calculation, it is found that when the flow rate of the pipeline with a barrier reaches 3 m/s, the Re is still laminar even if it has reached 8.2 × 10^6. In order to visually study the whole process of the transition of the drainage pipeline with a barrier, three greater flow rate conditions are added to the drainage pipeline with a barrier to make the transition process complete. According to the design conditions, a large number of examples in the range of Re = 10^3 − 2.73 × 10^8 are completed. The specific calculation conditions are shown in Table 4.

3. Analysis of Two-Dimensional Numerical Simulation Results

3.1. Typical Flow in Transition Process

In order to describe and understand the transition path of the multi-aperture basalt fiber drainage pipe convection system within the control parameter range, the bifurcation phenomenon that occurs in turn with the increase of Reynolds number will be described in detail and the corresponding mechanism will be discussed, and the formation mechanism will be analyzed in depth.

3.1.1. Steady Flow (Re < 1.09 × 10^8)

According to the 2D simulation results, it can be seen that the convection of multi-diameter basalt fiber drainage pipe is steady and symmetrical at small Reynolds number, that is to say, there is a stable symmetrical flow in the convection of multi-diameter basalt fiber drainage pipe, as shown in Figure 5. Under the small Reynolds number, the velocity structure of the multi-aperture basalt fiber drainage pipe is approximately mirror-symmetric about the x-axis of the central axis of the main pipe, and its flow is stable, and the velocity at each position does not change with time.

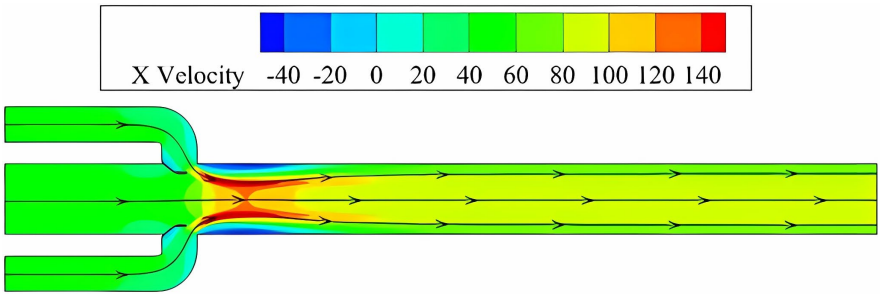

(a) X velocity cloud chart

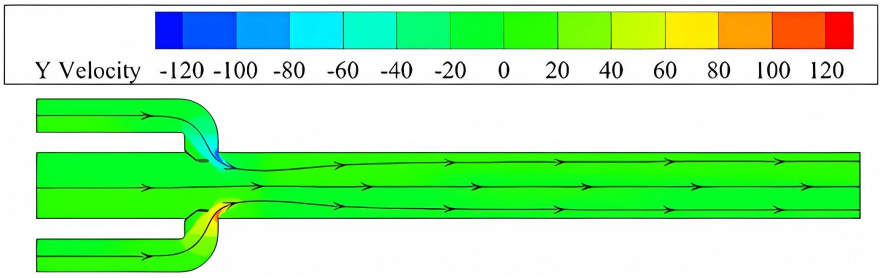

(b) Y velocity cloud chart

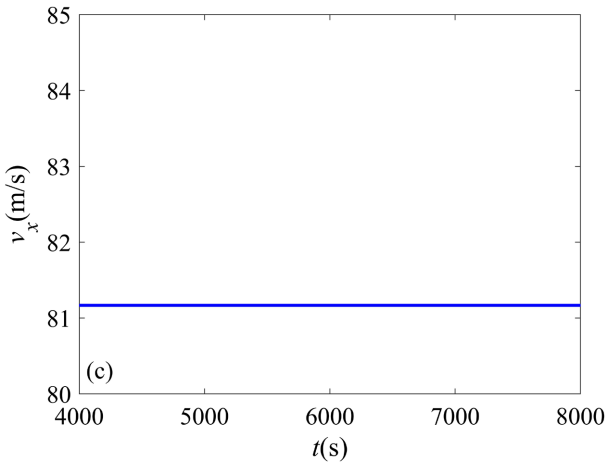

(c) Time series of the v_x at P_2

Figure 5. Multi-orifice basalt fiber drainage pipe convection Re = 1.09×10^8.

3.1.2. Pitchfork Bifurcation ($1.09 \times 10^8 \leq Re < 1.64 \times 10^8$)

The 2D numerical simulation results show that the steady flow of the multi-diameter basalt fiber drainage pipe can be maintained to Re < 1.09×10^8, and when Re = 1.64×10^8, the flow of the drainage pipe in the fully developed area of the space has evolved into an asymmetric structure. That is to say, when the Re is between 1.09×10^8 and 1.64×10^8, the fork bifurcation occurs, that is, the steady symmetric solution evolves into the steady asymmetric solution. In order to better observe the fork bifurcation, **Figure 6** shows the time series of velocity in different directions at the inner point P_2 (0, 0, 2.25) of the drainage pipe. It can be seen from the diagram that the array structure of velocity has been destroyed, and the results are completely opposite in the case of different Reynolds number approaching. The two results show a mirror symmetry structure.

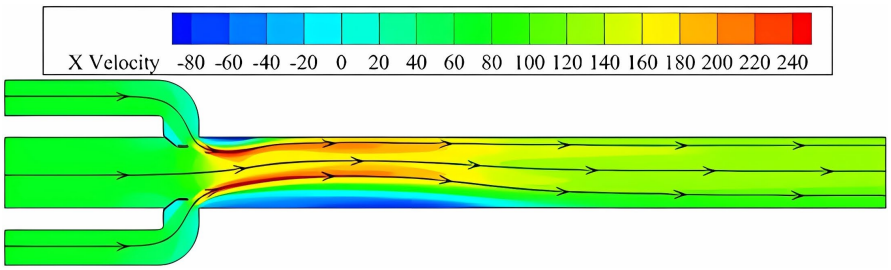

(a) The X velocity cloud chart of Re decreases approach

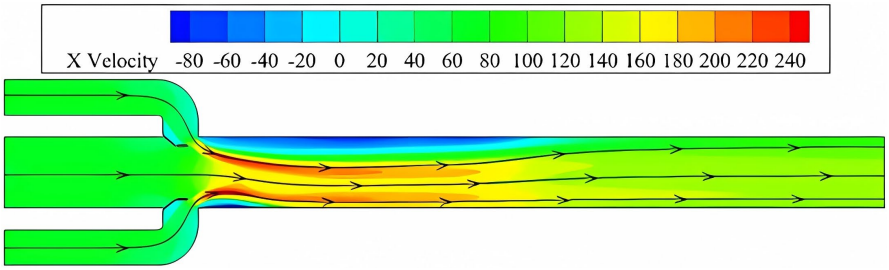

(b) The X velocity cloud chart of Re rising approach

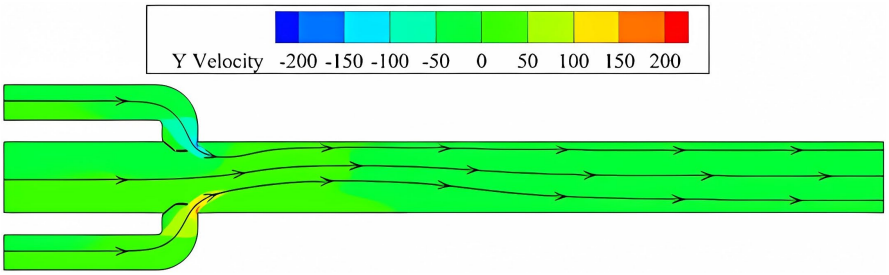

(c) The Y velocity cloud chart of Re decreases approach

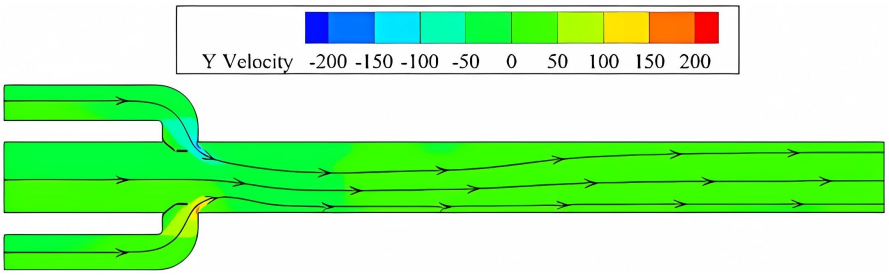

(d) The Y velocity cloud chart of Re rising approach

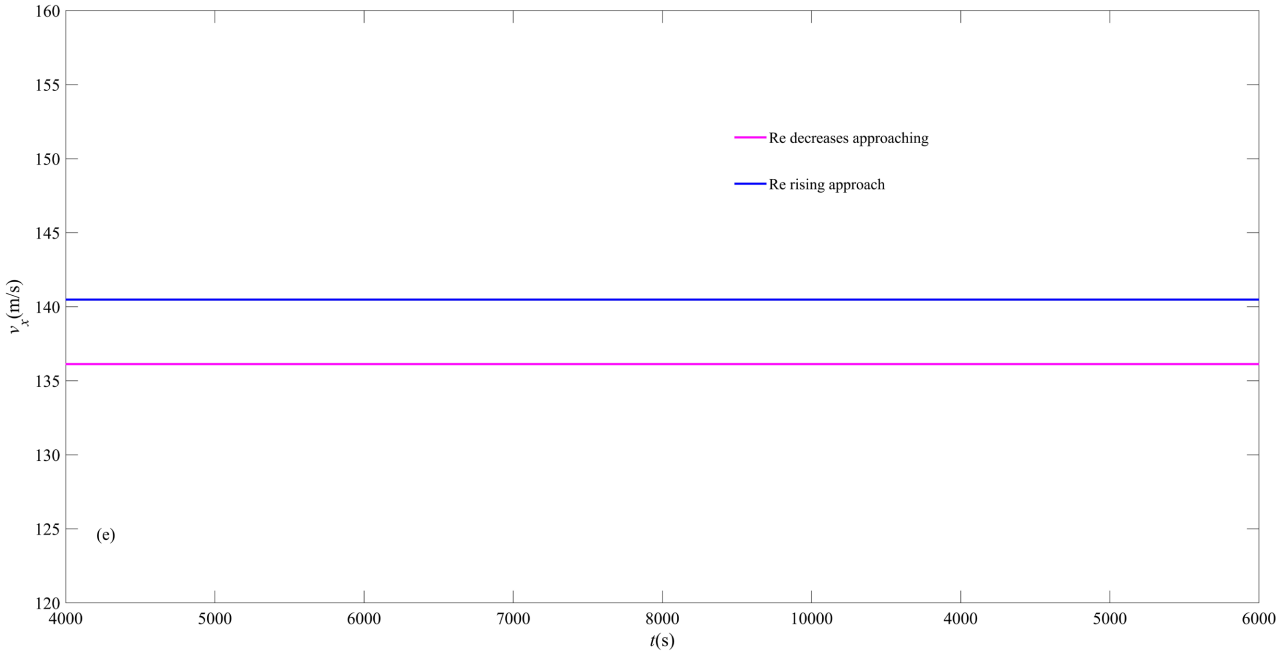

(e) X velocity-time curve of P_2

Figure 6. Multi-orifice basalt fiber drainage pipe convection Re = 1.64×10^8.

3.1.3. Chaotic Flow

The results of 2D numerical simulation show that with the further increase of Re, chaotic flow will occur in the multi-diameter fiber drainage pipe. In order to describe the chaotic flow characteristics, **Figure 7(a)** shows the Re = 2.73×10^8 isovelocity surface and streamline. It is clear that with the further increase of Re, the fluctuation along the y-direction is more obvious. At Re = 2.73×10^8, the velocity structure of the multi-diameter basalt fiber drainage pipe also loses the y-direction mirror symmetry about the central axis of the main pipe, see **Figure 7(b)**. **Figure 7(c)** and **Figure 7(d)** give the velocity time series and the corresponding spectrum of Re = 2.73×10^8. As shown in **Figure 7(d)**, the velocity time series with Re = 2.73×10^8 becomes chaotic, and its corresponding frequency has no clear peak frequency.

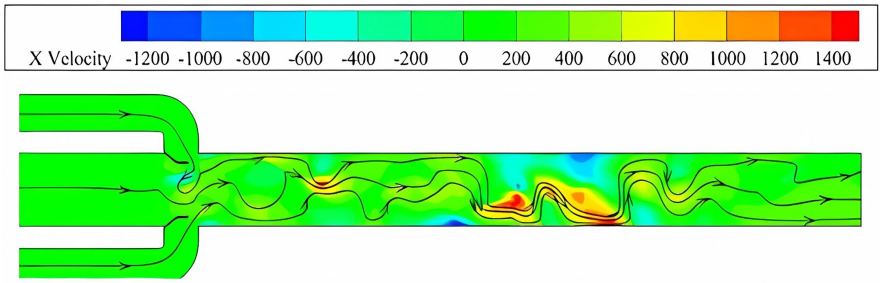

(a) X velocity cloud chart

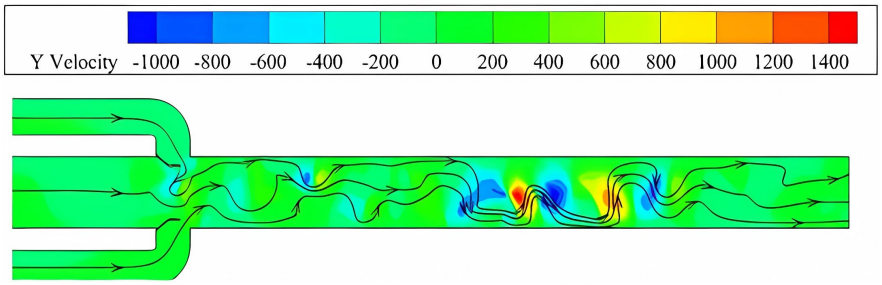

(b) Y velocity cloud chart

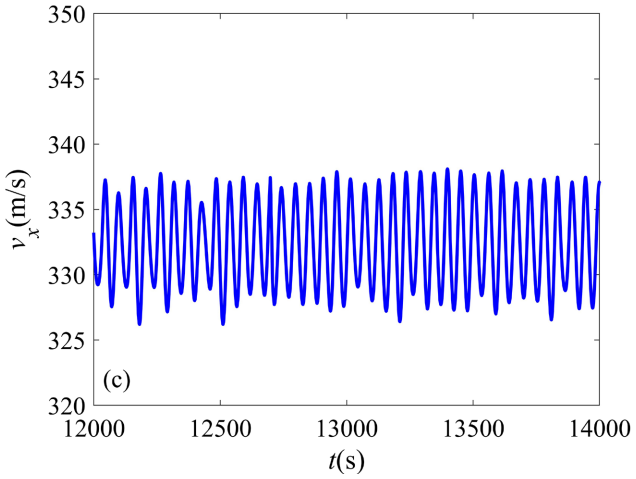

(c) X velocity-time curve of P_2

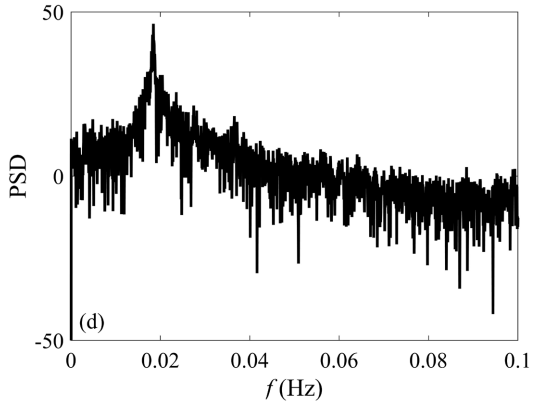

(d) power spectral density

Figure 7. Multi-orifice basalt fiber drainage pipe convection Re = 2.73×10^8.

3.2. Barrier Effect

According to the analysis of 2D numerical simulation results, the internal barrier of multi-diameter basalt fiber drainage pipe affects the transition path of convection in the pipe. **Figure 8** shows the comparison of the time series of the X velocity of P_2 under the condition of Re = 8.2×10^6 with or without barrier. It can be clearly seen from **Figure 8(a)** that the X velocity under the condition of Re = 8.2×10^6 with barrier is smaller than that without barrier. In addition, the velocity in the x direction fluctuates irregularly in the absence of a barrier, indicating that the flow enters a turbulent state, while the velocity in the x direction does not fluctuate in the presence of a barrier, indicating that the flow is a steady laminar flow. This indicates that the flow is more stable after the installation of the barrier, and the transition becomes turbulent later. It can be seen from **Figure 8(b)** that the Y velocity profile in the non-barrier pipe presents a Gaussian distribution, which is similar to the flow distribution in the straight pipe. After the installation of the barrier, the velocity profile in the y direction in the pipeline changes, the velocity distribution is more uniform than that without the barrier, the velocity on both sides is larger, and the flow mixing in the pipeline is more uniform.

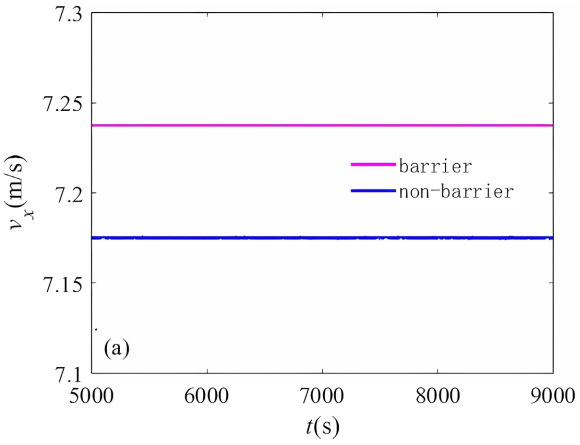

(a) The velocity-time curve of P_2

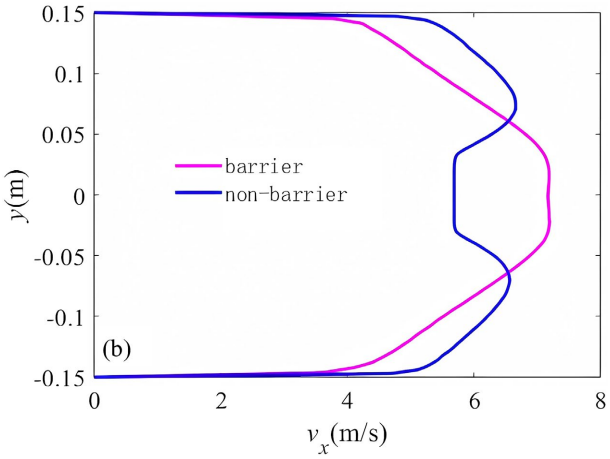

(b) Outlet velocity distribution curve

Figure 8. Re = 8.2×10^6.

According to the 2D numerical simulation results, the Reynolds number of the pipe flow in the multi-diameter basalt fiber drainage pipe is in the range of 10^3 ~ 2.73×10^8, and the flow pattern parameters in the drainage pipe with or without the barrier are shown in **Table 5**.

Table 5. Flow parameters of basalt drainage pipes.

Re	Flow pattern	
	Barrier	Non-barrier
$Re < 2.3 \times 10^3$	laminar flow	laminar flow
$2.3 \times 10^3 \leq Re < 8.2 \times 10^6$	laminar flow	turbulent flow
$8.2 \times 10^6 \leq Re \leq 1.09 \times 10^8$	laminar flow	-
$1.09 \times 10^8 < Re < 1.64 \times 10^8$	Pitchfork bifurcation	-
$Re \geq 2.73 \times 10^8$	turbulent flow	-

4. Conclusions

In this paper, a multi-diameter basalt fiber drainage pipe with a side main pipe diameter ratio of A_1:A_2 = 1:2 is selected as the research object. Water is used as the fluid medium, and the Prandtl number is Pr = 7. A large number of 2D numerical simulation analysis was carried out to study the transition path of the multi-diameter basalt fiber drainage pipe convection system in the $10^3 < Re < 2.73 \times 10^8$. The main conclusions are as follows:

1) The main mode solution of the multi-aperture basalt fiber drainage pipe convection system is a steady flow during the transition to chaos. The first fork bifurcation occurs at Re = 1.09×10^8 and Re = 1.64×10^8, and the flow field changes from steady symmetric flow to steady asymmetric flow. As the Re increases, when Re = 3.66×10^8, the flow evolves into chaotic flow.

2) Compared with the non-barrier, the transition process of the multi-aperture basalt fiber drainage pipe with barrier is significantly delayed, that is, the critical Re of the convective system in the drainage pipe from laminar flow to turbulent flow is larger, and the engineering benefit of the barrier design is significant.

3) Compared with the non-barrier, the installation of the barrier in the pipeline greatly reduces the fluctuation amplitude of the water flow along the gravity direction in the transition and turbulent states, and the radial mixing of the water flow along the pipeline is weakened, which effectively alleviates the water flow collision between the side nozzle and the main pipe, thus making the drainage of the pipeline more unobstructed after the confluence, reducing the head loss caused by the water flow collision, and significantly improving the water delivery efficiency of the pipeline.

The results show that the barrier can significantly improve the critical Re of the transition from the pipeline flow state to the chaotic flow, effectively reduce the energy loss of the water flow, and improve the water delivery efficiency of the pipeline. In the design of multi-diameter water pipelines, it is recommended to add a barrier at the confluence position.

Acknowledgments

The work was supported by Sichuan Science and Technology Program of China (No.2024ZHYS0001).

Declaration of Competing Interest

The authors declare that they have no known competing financial interests or personal relationships that could have appeared to influence the work reported in this paper.

Data Availability

Data will be made available on request.

Conflicts of Interest

The authors declare no conflicts of interest regarding the publication of this paper.

References

[1] Meseguer, Á. and Trefethen, L.N. (2003) Linearized Pipe Flow to Reynolds Number 107. *Journal of Computational Physics*, **186**, 178-197. https://doi.org/10.1016/s0021-9991(03)00029-9

[2] Manneville, P. (2017) Laminar-Turbulent Patterning in Transitional Flows. *Entropy*, **19**, Article No. 316. https://doi.org/10.3390/e19070316

[3] Tuckerman, L.S., Chantry, M. and Barkley, D. (2020) Patterns in Wall-Bounded Shear Flows. *Annual Review of Fluid Mechanics*, **52**, 343-367. https://doi.org/10.1146/annurev-fluid-010719-060221

[4] Keefe, L. (1998) Method and Apparatus for Reducing the Drag of Flows over Surfaces: US19960659306.

[5] Schlichting, H. (1991) Boundary Layer Theory Volume II. Translated by Xu, *et al.*, Science Press.

[6] Darbyshire, A.G. and Mullin, T. (1995) Transition to Turbulence in Constant-Mass-Flux Pipe Flow. *Journal of Fluid Mechanics*, **289**, 83-114. https://doi.org/10.1017/s0022112095001248

[7] Peixinho, J. and Mullin, T. (2006) Decay of Turbulence in Pipe Flow. *Physical Review Letters*, **96**, Article ID: 094501. https://doi.org/10.1103/physrevlett.96.094501

[8] Draad, A.A., Kuiken, G.D.C. and Nieuwstadt, F.T.M. (1998) Laminar-Turbulent Transition in Pipe Flow for Newtonian and Non-Newtonian Fluids. *Journal of Fluid Mechanics*, **377**, 267-312. https://doi.org/10.1017/s0022112098003139

[9] Peixinho, J. and Mullin, T. (2007) Finite-Amplitude Thresholds for Transition in Pipe Flow. *Journal of Fluid Mechanics*, **582**, 169-178. https://doi.org/10.1017/s0022112007006398

[10] Hattori, H., Wada, A., Yamamoto, M., Yokoo, H., Yasunaga, K., Kanda, T., *et al.* (2022) Experimental Study of Laminar-to-Turbulent Transition in Pipe Flow. *Physics of Fluids*, **34**, 1-18. https://doi.org/10.1063/5.0082624

[11] Kanda, T. (2016) Conservation-Law Approach for Transition in Pipe Flows. *Transactions of the Japan Society for Aeronautical and Space Sciences*, **59**, 356-363. https://doi.org/10.2322/tjsass.59.356

[12] Zagarola, M.V. and Smits, A.J. (1998) Mean-Flow Scaling of Turbulent Pipe Flow. *Journal of Fluid Mechanics*, **373**, 33-79. https://doi.org/10.1017/s0022112098002419

[13] Durst, F., Ray, S., Ünsal, B. and Bayoumi, O.A. (2005) The Development Lengths of Laminar Pipe and Channel Flows. *Journal of Fluids Engineering*, **127**, 1154-1160. https://doi.org/10.1115/1.2063088

[14] Nishi, M., Ünsal, B., Durst, F. and Biswas, G. (2008) Laminar-to-Turbulent Transition of Pipe Flows through Puffs and Slugs. *Journal of Fluid Mechanics*, **614**, 425-446. https://doi.org/10.1017/s0022112008003315

[15] Kühnen, J., Scarselli, D., Schaner, M. and Hof, B. (2018) Relaminarization by Steady Modification of the Streamwise Velocity Profile in a Pipe. *Flow, Turbulence and Combustion*, **100**, 919-943. https://doi.org/10.1007/s10494-018-9896-4

[16] Marensi, E., Willis, A.P. and Kerswell, R.R. (2019) Stabilisation and Drag Reduction of Pipe Flows by Flattening the Base Profile. *Journal of Fluid Mechanics*, **863**, 850-875.

[17] Marensi, E., Ding, Z., Willis, A.P. and Kerswell, R.R. (2020) Designing a Minimal Baffle to Destabilise Turbulence in Pipe Flows. *Journal of Fluid Mechanics*, **900**, A31. https://doi.org/10.1017/jfm.2020.518